Atmos. Meas. Tech. Discuss., 5, 5009–5041, 2012
www.atmos-meas-tech-discuss.net/5/5009/2012/
doi:10.5194/amtd-5-5009-2012

Atmospheric
Measurement
Techniques
Discussions

Evaluation of factors affecting accurate measurements of atmospheric CO_2 and CH_4 by wavelength-scanned cavity ring-down spectroscopy

H. Nara[1], H. Tanimoto[1], Y. Tohjima[1], H. Mukai[1], Y. Nojiri[1], K. Katsumata[1], and C. Rella[2]

[1]National Institute for Environmental Studies, 16-2 Onogawa, Tsukuba, Ibaraki 305-8506, Japan
[2]Picarro Inc., 3105 Patrick Henry Drive, Santa Clara California 94054, USA

Received: 22 June 2012 – Accepted: 2 July 2012 – Published: 20 July 2012

Correspondence to: H. Nara (nara.hideki@nies.go.jp)

Published by Copernicus Publications on behalf of the European Geosciences Union.

Title Page
Abstract | Introduction
Conclusions | References
Tables | Figures
◀| |▶
◀ ▶
Back | Close
Full Screen / Esc
Printer-friendly Version
Interactive Discussion

Abstract

We examined potential interferences from water vapor and atmospheric background gases (N_2, O_2, and Ar), and biases by isotopologues of target species, on accurate measurement of atmospheric CO_2 and CH_4 by means of wavelength-scanned cavity ring-down spectroscopy (WS-CRDS). Variations in the composition of the background gas substantially impacted the CO_2 and CH_4 measurements: the measured amounts of CO_2 and CH_4 decreased with increasing N_2 mole fraction, but increased with increasing O_2 and Ar, suggesting that the pressure-broadening effects (PBEs) increased as $Ar < O_2 < N_2$. Using these experimental results, we inferred PBEs for the measurement of synthetic standard gases. The PBEs were negligible (up to 0.05 ppm for CO_2 and 0.01 ppb for CH_4) for gas standards balanced with purified air, although the PBEs were substantial (up to 0.87 ppm for CO_2 and 1.4 ppb for CH_4) for standards balanced with synthetic air. For isotopic biases on CO_2 measurements, we compared experimental results and theoretical calculations, which showed excellent agreement within their uncertainty. We derived empirical correction functions for water vapor for three WS-CRDS instruments (Picarro EnviroSense 3000i, G-1301, and G-2301). Although the transferability of the functions was not clear, no significant difference was found in the water vapor correction values among these instruments within the typical analytical precision at sufficiently low water concentrations (< 0.3 %V for CO_2 and < 0.4 %V for CH_4). For accurate measurements of CO_2 and CH_4 in ambient air, we concluded that WS-CRDS measurements should be performed under complete dehumidification of air samples, or moderate dehumidification followed by application of a water vapor correction function, along with calibration by natural air-based standard gases or purified air-balanced synthetic standard gases with isotopic correction.

1 Introduction

Since atmospheric carbon dioxide (CO_2) is one of the most important trace gases in controlling the Earth's climate (e.g. surface temperature), much attention has been paid to the understanding of the global distribution of CO_2 during the last 50 yr of the twentieth century. Recent studies have pointed out that better understanding of non-CO_2 greenhouse gases (GHGs) is also needed to mitigate future climate change more effectively (Aydin et al., 2011; Kai et al., 2011; Montzka et al., 2011). Towards better and inclusive estimates of GHG emissions from terrestrial sources, top-down estimates by means of inverse model calculations are a key approach to decrease the uncertainty of bottom-up estimates, which are largely based on emission inventories. Ambient greenhouse gas observations have been extensively performed by a number of researchers using aircraft, ships, and ground-based stations. Although these observations have revealed detailed distributions of GHGs, ambient monitoring data are still sparse and less reliable in developing countries where GHG emissions are increasing rapidly due to increasing socioeconomic activities (Marquis and Tans, 2008). These studies point to the need for a comprehensive worldwide GHG observational system.

Ground- and satellite-based spectroscopic observation of GHGs is a powerful method to capture global distributions of GHGs. For example, the Total Carbon Column Observing Network (TCCON), a network of ground-based solar absorption Fourier transform infrared spectrometers, provides column abundances of CO_2, CH_4, N_2O, HF, CO, H_2O, and HDO at 18 sites (Wunch et al., 2012). Atmospheric Infrared Sounder (AIRS, which is mounted on the Aqua satellite) and the Scanning Imaging Absorption Spectrometer for Atmospheric Chartography (SCIAMACHY, which is mounted on the ENVISAT satellite; SCIAMACHY stopped its operation in May 2012 due to sudden communication blackout) provide global images of total column abundance of CO_2 and CH_4 (Buchwitz et al., 2005; Xiong et al., 2010). Analysis of CO_2 and CH_4 data obtained with the Greenhouse Gas Observing Satellite (GOSAT), launched on 23 January 2009 has begun recently (Heimann, 2009; Saitoh et al., 2009; Yokota et al., 2009; Yoshida et al., 2011). However, these satellite observations need to be supported by in-situ observations for validation and calibration of GHGs concentrations retrieved from observation data.

Originally developed by O'Keefe and Deacon (1988), cavity ring-down spectroscopy (CRDS) is a high-spectral-resolution, laser-based method for measuring the concentrations of gas-phase molecules with high precision and accuracy. The CRDS technique allows us to measure atmospheric trace gases on the basis of the decay rate of a laser confined in the optical cavity of the spectrometer. Since the initial development of the CRDS, this technique has been modified and applied to a variety of spectroscopic measurements of atmospheric trace gases (e.g. Brown, 2003). Wavelength-scanned (WS) cavity ring-down spectrometers manufactured by Picarro, Inc. (Santa Clara, CA) have been adopted with increasing frequency in GHG monitoring applications for detecting atmospheric CO_2, CH_4, and H_2O simultaneously (Crosson, 2008). The WS-CRDS instrument successfully fulfills increasing demands for scientists to expand routine monitoring at remote sites because the instrument is compact, lightweight, and easily maintained, resulting in excellent long-term stability with high precision and time resolution. For example, Chen et al. (2010) conducted airborne observations of CO_2 and CH_4 over the Amazon rain forest using a WS-CRDS instrument during the Balanço Atmosférico Regional de Carbono na Amazônia campaign in 2009. These investigators compared CO_2 measurements from a nondispersive infrared CO_2 analyzer (NDIR) and the WS-CRDS instrument, showing good agreement (within 0.05 ± 0.09 ppm) between the data obtained by means of the two methods. Beginning in April 2009, Winderlich et al. (2010) used the WS-CRDS instrument for continuous observations of CO_2 and CH_4 at a tall tower observation site (Zotino Tall Tower Observatory, established by Kozlova and Manning, 2009) in Central Siberia. Messerschmidt et al. (2011) used the WS-CRDS instrument in aircraft observational campaigns over European sites of the Total Carbon Column Observing Network to calibrate measurements of CO_2 and CH_4 column abundances obtained by satellite observations.

Chen et al. (2010) examined the analytical performance of a Picarro WS-CRDS instrument in detail. They showed that WS-CRDS measurements were affected by changes in the concentration of water vapor, background gases, and isotopologues of the target gas. Chen et al. also revealed some problems associated with WS-CRDS: for example, CO_2 and CH_4 measurements were substantially biased as a result of dilution and pressure-broadening due to the presence of water vapor. The investigators examined relationships between the dilution and pressure-broadening and the water vapor concentrations measured by WS-CRDS, suggesting that a single water vapor correction function can be applied universally to a given model of WS-CRDS instrument under the single calibration scale for the water vapor. In contrast, Winderlich et al. (2010) reported a water vapor correction function different from that reported by Chen et al. (2010), although the former group of investigators used a different WS-CRDS instrument (Picarro EnviroSense 3000i). These results suggest incompatibility of the correction function among different WS-CRDS models as well as differences in water vapor calibration scales. Chen et al. (2010) recommended the use of ambient air-based standard gas for WS-CRDS calibration to avoid possible biases due to variations in the mole fractions of background gases and the isotopologues of the target gases. However, the impact of such variations on the CO_2 and CH_4 measurements has not been tested quantitatively. For highly precise measurements of CO_2 and CH_4, the World Meteorological Organization recommends interlaboratory compatibilities of better than 0.1 ppm for CO_2 and 2 ppb for CH_4 (WMO, 2009). Thus, the factors affecting WS-CRDS measurements should be understood in detail and corrected if needed before data are shared by the community for inverse modeling work. In this study, we investigated Eq. (1) the impact of pressure-broadening effects (PBEs) caused by the background gases N_2, O_2, and Ar on synthetic standard gas measurement; Eq. (2) the correction for the isotopic bias on the CO_2 measurements through comparison between experimental results and theoretical calculations; and Eq. (3) the transferability of the water correction function among three WS-CRDS models manufactured by Picarro, Inc.

2 Wavelength-scanned cavity ring-down spectroscopy

In this study, we utilized three models of WS-CRDS instruments, the EnviroSense 3000i, G-1301, and G-2301, which are available from Picarro, Inc. (Santa Clara, CA, USA). Because detailed principles and the fundamental performance of the WS-CRDS instruments have been described elsewhere (Crosson, 2008), only a brief explanation is given here. The WS-CRDS can measure CO_2, CH_4, and H_2O simultaneously, operating on the principle of laser absorption spectroscopy. The WS-CRDS consists of a laser source, a high-precision wavelength monitor, a high-finesse optical cavity, a photodetector, and a data processing computer. An air sample is supplied into the optical cavity using a diaphragm pump while the pressure of the optical cavity is kept constant by adjusting the flow rate using two solenoid valves placed at the sample inlet and outlet of the cavity. A laser light at a specific wavelength from the light source is emitted into the optical cavity, and then the laser is shut off when the measurement signals from the photodetector achieve a steady-state condition. The optical cavity is equipped with three high-reflectivity mirrors ($> 99.995\,\%$) and has a volume of 40 ml (for the EnviroSense 3000i, the cavity volume is 35 ml). The cavity pressure and temperature are controlled rigorously at 140 ± 0.05 Torr and $40 \pm 0.01\,^{\circ}$C, respectively. The laser light confined in the cavity circulates among the three mirrors, resulting in an effective optical path length of about 20 km. The light intensity decays in time as the light leaks though the mirrors and is absorbed by target molecules. Because the difference in the decay (ring-down) time with and without laser absorption by the target molecule is proportional to the mole fraction of the target molecule in a sample gas, the mole fraction is calculated by monitoring the intensity of the leaking light in real time using the photodetector. The laser light is tightly tuned to scan the absorption spectral line of each target molecule: 1603 nm for $^{12}C^{16}O_2$ and 1651 nm for $^{12}CH_4$ and $H_2^{16}O$. Using the high-precision wavelength monitor, a high-resolution ($0.0003\,cm^{-1}$) absorption spectrum is obtained, allowing us to measure target gases accurately by minimizing interference from co-existing gases in the sample air. The WS-CRDS quantifies target gas mole fractions based on the gases' absorption peak maximum (so as peak height), and the absorption line-shapes of $^{12}C^{16}O_2$, $^{12}CH_4$, and $H_2^{16}O$ are modeled by fitting with a Galatry function (Galatry, 1961). The typical analytical precision of CO_2 and CH_4 measurements obtained by the WS-CRDS instruments used in this study were very similar: 0.04 ppm and 0.3 ppb for EnviroSense 3000i, 0.05 ppm and 0.3 ppb for G-1301, 0.03 ppm and 0.3 ppb for G-2301, respectively.

3 Pressure-broadening effects of background gases

Past studies revealed that infrared spectroscopic analysis of CO_2 using NDIR is biased depending on the different types of NDIR instrument by change of temperature, pressure, and matrix gas composition (Bischof, 1975; Perman and Garratt, 1975; Griffith, 1982; Griffith et al., 1982). This bias results from absorption line-broadening and -narrowing of CO_2 molecule due to random thermal motion of the molecules, collisions between molecules, and velocity-changing collisions (Varghese and Hanson, 1984). Random thermal motion and intermolecular collisions produce line-broadening effects (referred to as Doppler and Lorentzian broadening effects, respectively), while the velocity-changing collisions produce line-narrowing effects (a kind of Dicke narrowing), which diminish the Doppler broadening effects (Dicke, 1953).

The WS-CRDS models the absorption line-shape of the target gases using the Galatry function, which describes the above-mentioned line-broadening and -narrowing effects simultaneously (Galatry, 1961). In the Galatry function, the Doppler and Lorentzian broadening effects and the line-narrowing effects are parameterized as the variables x, y, and z, respectively, and the function is represented by these three variable parameters (Varghese and Hanson, 1984). For WS-CRDS measurements, the Galatry line-shape is determined by the line-width parameters y and z because the Doppler broadening effect (x), when expressed as a function of temperature, can be considered a constant value in a well-controlled optical cavity. The magnitudes of Lorentzian broadening (y) and the line-narrowing effect (z) are intrinsic properties of the target molecule are affected only by the matrix gas composition in WS-CRDS measurement while the areas of the absorption line-shapes remained unchanged. Because the line-narrowing effect is of much smaller magnitude than Lorentzian broadening, we hereafter refer to both effects collectively as PBEs.

Despite precise modeling of line-shape of target gases by the Galatry function, the WS-CRDS measurements are biased by these line-broadening and -narrowing effects when the sample and calibration gas matrix differ in their composition due to the dependency of line-width parameters y and z on the matrix gas composition. Because the WS-CRDS quantifies target gases based on the absorption peak maximum in order to obtain excellent long-term stability and high precision (Rella, 2010), change in the line-shape resulting from the variation of these line-width parameters leads to over and underestimation of target gases. In fact, Chen et al. (2010) reported significant line-broadening effects during the measurement of synthetic standard gases by WS-CRDS calibrated with ambient air.

If we assume that PBEs are linearly proportional to infinitesimal changes in the matrix gas composition, we can approximate the magnitude of PBEs on CO_2 and CH_4 absorption spectral lines. For multicomponent gas mixtures, line-width parameters y and z for the specific spectral absorption lines of the target gases in the mixture are given by the sum of the pure gas line-width parameters weighted by each gas's mole fraction in the mixture. For atmospheric observation, the line-width parameters y and $z$are subject to background gases (N_2, O_2, and Ar), and thus the effective line parameters y_{eff} and z_{eff} are expressed as follows:

$$\begin{aligned} y_{\text{eff}} &= c_{N_2} y_{N_2} + c_{O_2} y_{O_2} + c_{\text{Ar}} y_{\text{Ar}} \\ z_{\text{eff}} &= c_{N_2} z_{N_2} + c_{O_2} z_{O_2} + c_{\text{Ar}} z_{\text{Ar}}, \end{aligned} \tag{1}$$

where c is mole fraction for the background gas indicated as subscript. The variations of the background gases in the atmosphere are usually small enough to approximate the Galatry function by a two-dimensional Taylor expansion about y_{eff} and z_{eff} given for nominal atmospheric composition:

$$G(y+\Delta y_{\mathrm{eff}}, z+\Delta z_{\mathrm{eff}}) = G(y,z) + \frac{\partial}{\partial y}G(y,z)\Delta y_{\mathrm{eff}} + \frac{\partial}{\partial z}G(y,z)\Delta z_{\mathrm{eff}}. \tag{2}$$

G expresses maximum value of line-shape function defined by the Galatry function with line-width parameters y and z at measured wavelength (1603 nm for CO_2, 1651 nm for CH_4), and Δy_{eff} and Δz_{eff} are defined by Eq. (1) corresponding to infinitesimal changes of the background gases. Equation (2) is then rearranged to

$$\frac{G(y+\Delta y_{\mathrm{eff}}, z+\Delta z_{\mathrm{eff}}) - G(y,z)}{G(y,z)} = k_y \Delta y_{\mathrm{eff}} + k_z \Delta z_{\mathrm{eff}}, \tag{3}$$

where

$$\begin{aligned} k_y &= \frac{1}{G(y,z)}\frac{\partial}{\partial y}G(y,z) \\ k_z &= \frac{1}{G(y,z)}\frac{\partial}{\partial z}G(y,z). \end{aligned} \tag{4}$$

From Eqs. (1) and (3), we obtain the following equation:

$$\begin{aligned} \mathrm{PBE} &= \frac{G(y+\Delta y_{\mathrm{eff}}, z+\Delta z_{\mathrm{eff}}) - G(y,z)}{G(y,z)} \times c_{\mathrm{target}} \\ &= c_{\mathrm{target}}\{(k_y y_{N_2} + k_z z_{N_2})\delta c_{N_2} + (k_y y_{O_2} + k_z z_{O_2})\delta c_{O_2} + (k_y y_{\mathrm{Ar}} + k_z z_{\mathrm{Ar}})\delta c_{\mathrm{Ar}}\}, \end{aligned} \tag{5}$$

PBE indicates the magnitude of PBEs on the target gas (units corresponding to that of the target gas); c_{target} is the mole fraction of the target gas (in ppm for CO_2 and in ppb for CH_4); δc indicates variation of the inert gas indicated as subscript from its nominal composition. Here we define a dimensionless pressure-broadening coefficient ε per target gas mole fraction to express $(k_y y_i + k_z z_i)$. We then rearrange Eq. (5) using ε:

$$\mathrm{PBE}/c_{\mathrm{target}} = \varepsilon_{N_2}\delta c_{N_2} + \varepsilon_{O_2}\delta c_{O_2} + \varepsilon_{\mathrm{Ar}}\delta c_{\mathrm{Ar}}. \tag{6}$$

Among each inert gas, following approximation holds as:

$$\delta c_{N_2} + \delta c_{O_2} + \delta c_{Ar} \approx 0. \quad (7)$$

By eliminating δc_{N_2} in Eq. (6) using the relation expressed as Eq. (7), we obtain following equation:

$$\mathrm{PBE}/c_{\mathrm{target}} = \Delta\varepsilon_{O_2}\delta O_2 + \Delta\varepsilon_{Ar}\delta Ar, \quad (8)$$

where $\Delta\varepsilon_{O_2}$ and $\Delta\varepsilon_{Ar}$ are delta coefficients, defined as the difference between the pressure-broadening coefficient of O_2 or Ar from that of N_2. Thus PBEs can be estimated from the empirical relationship between PBEs and matrix gas variations. In the next section, we examine this empirical relationship in the context of CO_2 and CH_4 measurements obtained in a series of experiments.

3.1 Relationship between matrix gas composition and pressure-broadening effects

The effects of pressure-broadening due to changes in the matrix gas composition on CO_2 and CH_4 measurements were examined using a dynamic gas blending unit (Fig. 1). The unit consists of two sets of high-pressure cylinders, thermal mass flow controllers, and precise flow meters, and the three WS-CRDS instruments. In the experiments, compressed air and high-purity inert gas (> 99.9999 % N_2, O_2, or Ar, Japan Fine Products, Inc., Kanagawa, Japan) from these two high-pressure cylinders were dynamically mixed at a certain blending ratio by controlling their flow rates with the mass flow controllers (model 3660, Kofloc, Tokyo, Japan, for compressed air control; model SEC-E40, Horiba Stec, Tokyo, Japan, for pure inert gas control), which were calibrated precisely by means of the high-precision flow meters (molbloc/molbox flow calibration system, DH Instruments, Inc., Phoenix, AZ, USA). The mixed sample flow was supplied to the WS-CRDS instruments (models EnviroSense 3000i, G-1301, and G-2301) for quantification of the target gases. The mole fractions of the target gases were calculated as the average values observed over a period of 5 min after the sample signals stabilized.

As mentioned above, the individual pure inert gases were obtained commercially; the compressed air was prepared in our laboratory using ambient air collected outside the laboratory. This ambient air was dehumidified by passing through a Nafion Permapure dryer (PD-200T-24, Japan Controls Co., Tokyo, Japan) and a chemical trap packed with phosphorus pentoxide (P_2O_5, 20/48 mesh, Wako Pure Chemical Industries, Osaka, Japan). The dew point of the dehumidified ambient air was less than $-80\,^{\circ}$C. Calibrated by means of NDIR and gas chromatography/flame ionization detection with reference to the National Institute for Environmental Studies standard gas scale (Machida et al., 2007), the mole fractions of CO_2 and CH_4 in the compressed air were 402.26 ppm and 1917.57 ppb, respectively. Typical analytical precisions ($\pm 1\sigma$) for CO_2 and CH_4 were 0.03 ppm and 1.7 ppb, respectively. The background gas composition of the compressed air was determined by measuring the O_2 mole fraction according to the method developed by Tohjima et al. (2000) under the assumption that the Ar mole fraction in the compressed air was identical to that in the atmosphere. We defined the background gas mole fractions in ambient air as $N_2 = 0.780876$, $O_2 = 0.209392$, and $Ar = 0.009333$ (Tohjima et al., 2005).

The magnitudes of PBEs due to changes in the matrix gas composition can be calculated as:

$$\mathrm{PBE} = \Delta c - D, \qquad (9)$$

where Δc and D indicate the observed variations in the mole fraction of the target gases and dilution effects on the target gases owing to the addition of the inert gases, respectively. The dilution effects in Eq. (9) were also calculated from the mole fractions of the target gases and the flow rates of the compressed air and pure inert gas:

$$D = c_0 \times \left(1 - \frac{F_{\mathrm{comp}}}{F_{\mathrm{comp}} + F_{\mathrm{inert}}}\right), \qquad (10)$$

where c_0 is the original mole fraction of the target gas before blending with the inert gas. The variables F_{comp} and F_{inert} indicate the flow rates of the compressed air and the inert gas, respectively. Using Eqs. (9) and (10), PBEs are calculated from following equation.

$$\text{PBE} = \Delta c - c_0 \times \left(1 - \frac{F_{\text{comp}}}{F_{\text{comp}} + F_{\text{inert}}}\right). \tag{11}$$

We examined PBEs on CO_2 and CH_4 by increasing the mixing ratios of N_2, O_2, and Ar in the sample air from their natural levels to 2.5, 8.8, and 27.7 %, respectively. A linear behavior in PBEs for both CO_2 (Fig. 2) and CH_4 (Fig. 3) was observed with increasing inert gas mole fraction in the sample air within the investigated range for the three WS-CRDS instruments; the linear behavior depended on the inert gas species. For example, N_2 addition resulted in an apparent decrease of CO_2, whereas O_2 and Ar addition resulted in an apparent increase of CO_2. For a 2.5 % increase of N_2, O_2, and Ar, G-1301 showed apparent CO_2 and CH_4 variations of −0.93, +0.23, and +0.01 ppm and −1.08, +0.22, and +0.02 ppb, respectively. These results suggest that PBEs generated by these inert gases are expressed as linear functions with respect to variations of the matrix gas composition for both CO_2 and CH_4. Furthermore, the apparent variations of CO_2 and CH_4 indicate that N_2 imparts the greatest PBE followed by O_2, whereas Ar imparts the smallest PBE.

Nakamichi et al. (2006) investigated PBEs of pure inert gases, including N_2, O_2, and Ar, for rotational transitions in the $(3\ 0^0\ 1)_{III} \leftarrow (0\ 0\ 0)$ band of CO_2 at around 1600 nm within the temperature range 263–326 K. They observed a linear PBE response with increasing inert gas, and the obtained pressure-broadening coefficients decreased in the order $N_2 > O_2 > \text{Ar}$. For example, the pressure-broadening coefficient (unit: γ cm^{-1} atm^{-1}) for CO_2 at 298 K was 0.078 for N_2, 0.067 for O_2, and 0.062 for Ar (Nakamichi et al., 2006). Our experimental results agree reasonably well with those published results.

From our results, we calculated the delta coefficients for CO_2 and CH_4 according to Eq. (8) by a linear least-squares analysis (Table 1). Based on these delta coefficients, the linear relationship between the background gas composition and PBEs was calculated. The calculated linear relationship reproduced the experimental results well (Figs. 2 and 3), suggesting that PBEs resulting from variations in background gas composition can be approximated by Eq. (8). Although different delta coefficients were obtained among the WS-CRDS instruments, no significant differences were found in the PBE calculations among these instruments in the present work. Hereafter we focus on the results from G-1301 as a representative case.

3.2 Pressure-broadening effects for the synthetic standard gas measurements

As an example, we estimated the PBEs for CO_2 at 400 ppm and for CH_4 at 2000 ppb in response to O_2 and Ar variations for G-1301 (Fig. 4). Here we calculated PBEs from −20 000 to +20 000 ppm relative to the ambient O_2 level and from zero to +7000 ppm relative to the ambient Ar level. The estimated PBEs corresponded to variations in target gas measurements from about −1.6 to +1.5 ppm for CO_2 and from −2.3 to +2.0 ppb for CH_4.

As a model case, we inferred the magnitude of possible PBEs during the measurement of a synthetic standard gas produced by Japan Fine Products. According to Japan Fine Products, the relative error for the O_2 and Ar mole fractions in N_2-balanced N_2/O_2/Ar synthetic air is guaranteed within ±5 % from the nominal atmospheric O_2 and Ar mole fractions, and the O_2 mole fraction is guaranteed within ±2 % for N_2-balanced N_2/O_2 synthetic air. On the basis of these production errors, we can restrict the PBEs from ±0.51 ppm for CO_2 and from −0.69 to +0.57 ppb for CH_4 for our measurements of standard gases diluted with the N_2/O_2/Ar synthetic air. On the other hand, PBEs for the standard gas with N_2/O_2 synthetic air are restricted to be from about −0.50 to −0.87 ppm for CO_2 and from −1.4 to −1.0 ppb for CH_4.

To prevent possible PBEs derived from variations in matrix gas composition, purified air is the preferred balance gas to be used for gas standards for WS-CRDS because purified air is expected to have the same background gas composition of N_2, O_2, and Ar as that found in ambient air. Japan Fine Products uses ambient air to produce purified air, in which H_2O and atmospheric trace gases (such as CO_2 and CH_4) are removed by cryogenic separation. After the cryogenic separation, any remaining impurities in the processed air are removed by passing the air through columns packed with a heated Pt catalyst and molecular sieves (Tohjima et al., 2009). During these purification processes, O_2 can be removed from the processed air due to the oxidation of organic compounds and to strong absorption onto the molecular sieves when the sieves are fresh condition, although N_2 and Ar are not absorbed at significant levels by the sieves. We have often checked the O_2 mole fraction in purified air from Japan Fine Products by means of N_2/O_2 ratio analysis (Tohjima et al., 2005), which has revealed that O_2 decreases from ambient levels empirically by 1000 ppm, at most. In this case, the PBEs derived from the O_2 decrease are estimated to be up to −0.05 ppm for CO_2 and −0.01 ppb for CH_4, which are negligible effects.

4 Isotope correction for CO_2 measurements

As was reported by Chen et al. (2010), WS-CRDS measurements are biased due to the difference in the fractional abundance of each isotopologue of a target gas between the calibration gas and air sample: WS-CRDS determines the mole fraction of a target gas by evaluating only the main isotopologue of the target gas (e.g. $^{12}C^{16}O^{16}O$ for CO_2 measurements) in the air sample, under the assumption that the fractional abundances of minor isotopologues in the air sample are the same as those in the calibration gas.

The fractional abundance of each isotopologue can be calculated from stable isotopic analysis. Since variation in the stable isotope abundance of a specific element is usually very small, the isotope abundance is expressed as a deviation from a defined standard material in permil (‰) using delta notation. For example, stable carbon isotope ratio is defined as follows:

$$\delta^{13}\mathrm{C} = \left[\frac{{}^{13}R_{\mathrm{sam}}}{{}^{13}R_{\mathrm{ref}}} - 1\right] \times 1000\,‰, \tag{12}$$

where ${}^{13}R_{\mathrm{sam}}$ and ${}^{13}R_{\mathrm{ref}}$ is absolute ratio of ^{13}C and ^{12}C abundance ^{13}C/^{12}C for a sample and a reference material, respectively. Similarly, stable oxygen isotope ratio is defined as

$$\delta^{18}\mathrm{O} = \left[\frac{{}^{18}R_{\mathrm{sam}}}{{}^{18}R_{\mathrm{ref}}} - 1\right] \times 1000\,‰. \tag{13}$$

For stable carbon and oxygen isotopic analysis, Vienna Pee Dee Belemnite (VPDB) and Vienna Standard Mean Ocean Water (VSMOW) are referenced as standard materials.

Chen et al. (2010) derived an isotopic correction equation for CO_2 measurements by WS-CRDS instrument due to the difference of δ^{13}C and δ^{18}O values of CO_2 in ambient air ($\delta^{13}\mathrm{C}_{\mathrm{amb}}$, $\delta^{18}\mathrm{O}_{\mathrm{amb}}$) from those in synthetic standard gas ($\delta^{13}\mathrm{C}_{\mathrm{syn}}$, $\delta^{18}\mathrm{O}_{\mathrm{syn}}$) according to following equation:

$$\mathrm{CO}_{2\,\mathrm{amb}} = \mathrm{CO}_{2\,\mathrm{CRDS}} \times \left[\frac{1 + {}^{13}R_{\mathrm{ref}} \times (1 + \delta^{13}\mathrm{C}_{\mathrm{amb}}) + 2 \times {}^{18}R_{\mathrm{ref}} \times (1 + \delta^{18}\mathrm{O}_{\mathrm{amb}})}{1 + {}^{13}R_{\mathrm{ref}} \times (1 + \delta^{13}\mathrm{C}_{\mathrm{syn}}) + 2 \times {}^{18}R_{\mathrm{std}} \times (1 + \delta^{18}\mathrm{O}_{\mathrm{syn}})}\right], \tag{14}$$

where $\mathrm{CO}_{2\,\mathrm{amb}}$ and $\mathrm{CO}_{2\,\mathrm{CRDS}}$ are the CO_2 mole fraction in ambient air and the CO_2 value determined by WS-CRDS, respectively. The researchers calculated the isotopic biases based on reported δ^{13}C and δ^{18}O values typically found for CO_2 in synthetic standard gases ($\delta^{13}\mathrm{C} = -37 \pm 11\,‰$ vs. VPDB, and $\delta^{18}\mathrm{O} = 24 \pm 10\,‰$ vs. VSMOW) (Coplen et al., 2002) and background atmosphere ($\delta^{13}\mathrm{C} = -8\,‰$ vs. VPDB, $\delta^{18}\mathrm{O} = 42\,‰$ vs. VSMOW) (GLOBALVIEW-CO2C13, 2009; Allison and Francey, 2007). The resulting calculated biases were from 0.14 to 0.16 ± 0.06 ppm.

Although isotopic correction for CH_4 was not reported by Chen et al. (2010), we roughly calculated the correction value by referencing past studies. Here stable hydrogen isotope ratio (δD) is defined as similar to that of carbon and oxygen:

$$\delta D = \left[\frac{{}^{2}R_{\mathrm{sam}}}{{}^{2}R_{\mathrm{ref}}} - 1 \right] \times 1000\,‰, \tag{15}$$

where ${}^{2}R_{\mathrm{sam}}$ and ${}^{2}R_{\mathrm{ref}}$ is D/H ratio for a sample and reference material. The δD value is also normalized to the VSMOW scale. For the methane measurements, isotopic correction equation is given as:

$$CH_{4\,\mathrm{amb}} = CH_{4\,\mathrm{CRDS}} \times \left[\frac{1 + {}^{13}R_{\mathrm{ref}} \times (1 + \delta^{13}C_{\mathrm{amb}}) + 4 \times {}^{2}R_{\mathrm{ref}} \times (1 + \delta D_{\mathrm{amb}})}{1 + {}^{13}R_{\mathrm{ref}} \times (1 + \delta^{13}C_{\mathrm{syn}}) + 4 \times {}^{2}R_{\mathrm{std}} \times (1 + \delta D_{\mathrm{syn}})} \right]. \tag{16}$$

If we assume that typical $\delta^{13}C$ and δD values of synthetic CH_4 are close to those for fossil fuel production of -40 ± 7 ‰ for $\delta^{13}C$ (VPDB) and -175 ± 10 ‰ for δD (VSMOW) (Snover et al., 2000), and if we use $\delta^{13}C$ and δD values for ambient CH_4 in northern hemispheric pristine air of -47.4 ± 0.1 ‰ for $\delta^{13}C$ (VPDB) and -91 ± 5 ‰ for δD (VSMOW) (Quay et al., 1999), the correction value is estimated according to Eq. (16) to be about 0.06–0.07 ± 0.3 ppb depending on the mixing ratios of CH_4. Taking into account the typical analytical precision of a WS-CRDS instrument (±0.3 ppb), this result indicates that the isotopic bias for CH_4 measurements is not significant. We therefore examined the correction value only for CO_2 measurements.

We assessed the CO_2 isotopic correction method through comparison between the experimentally determined isotopic biases and theoretically calculated isotopic collection values according to Eq. (14). The isotopic biases were estimated from the difference in CO_2 measurements between WS-CRDS and NDIR. For the comparison, we prepared three CO_2-in-air high-pressure cylinders as sample gases and six high-pressure cylinders for instrumental calibration. The three sample cylinders consisted of compressed natural air and a mixture of pure CO_2, having different mole fractions and stable isotope ratios, and purified air. The mole fraction and stable carbon and oxygen isotope ratios of CO_2 in these sample cylinders are listed in Table 2. For the calibration gas, each high-pressure cylinder contained a different CO_2 mole fraction (350.35, 359.89, 370.22, 389.04, 419.78, or 429.59 ppm) with similar stable isotope ratios ($\delta^{13}C = -29.64 \pm 0.22$ ‰ vs. VPDB, $\delta^{18}O = -27.53 \pm 1.09$ ‰ vs. VPDB). Following the method of Tohjima et al. (2009), isotopic biases for the NDIR measurements were corrected precisely using the same NDIR instrument after the determination of stable carbon and oxygen isotope ratios by a conventional isotope ratio mass spectrometer (Finnigan MAT 252, ThermoQuest, Bremen, Germany) with dual inlets. PBEs for the WS-CRDS measurements were also corrected using our experimental results, while the background gas composition was determined according to the method reported by Tohjima et al. (2000).

As an example, the CO_2 mole fractions, isotopic values, and their correction values from NDIR and the WS-CRDS instrument (G-1301) for three standard gas samples are summarized in Table 2 along with theoretically calculated isotopic correction values. The experimentally determined isotopic biases agreed well with the calculated correction values within the experimental errors, suggesting no significant differences between these two methods. From these results, we have demonstrated that isotopic biases for CO_2 measurements can be corrected according to the method by Chen et al. (2010) using isotopic values of CO_2.

5 Water correction functions for three different WS-CRDS models

We determined the water correction functions for the three WS-CRDS instruments under the same experimental conditions using the above-mentioned humidification system (Fig. 1). In this experiment, we used the same compressed ambient air prepared for the gas blending experiments (see Sect. 3.1). The compressed air was introduced into the WS-CRDS instruments through a dew point generator (model LI-610, Li-Cor, Inc., Lincoln, NE, USA) for sample humidification while the excess flow was exhausted through the chilled mirror dew point hygrometer (model DPH-503H, Tokyo Opto-Electronics Co., Ltd.) for the calibration of water vapor measurements by the WS-CRDS instruments. The humidified air sample was supplied to the WS-CRDS instruments for 5 min with and without passing through a two-step dehumidification unit, which consisted of an electric cooler (thermoelectric dehumidifier, DH-109, Komatsu Electronics Inc., Kanagawa, Japan) and a chemical trap filled with magnesium perchlorate (20/48 mesh, Wako Pure Chemical Industries, Osaka, Japan), making the dew point of the humid air sample less than −50 °C. To correct CO_2 drifts due to changes in the solubility of CO_2 in the water pool of the humidifier, dry or humidified air was supplied to the WS-CRDS instruments alternately as reported by past studies (Chen et al., 2010; Winderlich et al., 2010); no significant variations in the solubility of CH_4 were observed.

We examined the WS-CRDS response for CO_2 and CH_4 at water vapor concentrations of 0.16 to 4.42 %V (% by volume) (Fig. 5). In the water vapor range examined here, the wet to dry ratio (wet/dry) of the target gas mixing ratio decreased to about 0.94 for CO_2 and 0.95 for CH_4, corresponding to a decrease of 25 ppm and 95 ppb, respectively. The water correction function was determined from the relationship between the WS-CRDS reading of the water vapor concentrations and the wet/dry ratios for CO_2 and CH_4 by second-order polynomial fitting in order to correct the impact of self-broadening effect of water vapor itself (Chen et al., 2010):

$$\frac{X_{\mathrm{wet}}}{X_{\mathrm{dry}}} = 1 - a \cdot [\mathrm{H_2O}]_{\mathrm{CRDS}} - b \cdot [\mathrm{H_2O}]^2_{\mathrm{CRDS}}, \tag{17}$$

where $[H_2O]_{CRDS}$ indicates water vapor concentration reported by the WS-CRDS instrument. Estimated linear (a) and quadratic (b) terms in Eq. (17) are listed in Table 3. The residuals from the fitting curve were within ±0.08 ppm and ±0.8 ppb for CO_2 and CH_4, respectively (Fig. 5). All the coefficients of determination (R^2) for both CO_2 and CH_4 from individual WS-CRDS instruments were greater than 0.999.

Although our estimates for the three WS-CRDS instruments were very close to one another, and also in good agreement with those obtained from past studies (Chen et al., 2010; Winderlich et al., 2010), these water correction functions provided significantly different water correction values depending on the water vapor concentrations. Chen et al. (2010) reported that the water vapor measurements of the two WS-CRDS instruments used in that study were different due to the difference in the water vapor calibration scales between the instruments. To evaluate the transferability of the water correction functions precisely, the water vapor measurements obtained from the WS-CRDS instruments were calibrated on the basis of the dew point measurements. After the calibration, we compared the water correction values from the individual correction functions (Fig. 6). Because of large experimental uncertainty due to CO_2 drift corrections resulting from the temperature-dependent variation in CO_2 dissolution in the water pool, as well as the uncertainty associated with the water vapor calibration method, no significant differences in water correction values among these different instruments were observed whereas the differences can be obscured by these uncertainties. More precise experiments than these may be needed to scrutinize the compatibility of the water correction function among instrument models; however, such highly precise experiments are difficult to carry out.

Although the transferability of water correction functions between different instrument models is not clear from our experiments, we concluded that the difference between the correction functions was negligible at lower water vapor concentrations for all WS-CRDS models tested: the differences among the three WS-CRDS instruments were within the typical analytical precision ($\pm 1\sigma$) at calibrated water vapor concentrations of < 0.3 %V for CO_2 and < 0.4 %V for CH_4. Taking into account that lack of a water vapor standard material prevents WS-CRDS measurements from being performed under exactly the same water vapor calibration scale among different laboratories, we concluded that complete dehumidification or moderate dehumidification followed by application of a water correction function is the best strategy to remove measurement biases from dilution, PBEs, and water vapor calibration, thus enabling accurate CO_2 and CH_4 measurements.

6 Conclusions

We investigated factors affecting WS-CRDS measurement, including effects from pressure broadening of the background gases' spectral lines, variations in isotopologues of the target gases, and vapor dilution and pressure broadening of water vapor. Using a dynamic gas blending system, we determined the delta coefficients, defined as the difference in the pressure-broadening coefficients of O_2 and Ar from the coefficient of N_2, by linear least-squares analysis. On the basis of the calculated delta coefficients, we inferred the magnitude of possible PBEs associated with the measurement of synthetic standard gases supplied by Japanese gas manufacturer as a model case. The magnitudes of the PBEs were classified into three cases depending on the background gas. For the preparation of N_2-balanced N_2/O_2/Ar and N_2/O_2 synthetic air, the relative error for O_2 and Ar mole fraction is guaranteed ±5 % and ±2 % from their nominal composition. The corresponding PBEs impact on CO_2 and CH_4 were estimated to be up to about ±0.5 ppm and ±0.7 ppb for the former synthetic air, and from −0.49 to −0.87 ppm and from −1.4 to −1.0 ppb for the latter one, respectively. In contrast, the PBEs for purified air were estimated to be up to −0.05 ppm for CO_2 and −0.01 ppb for CH_4 on the basis of our O_2 analysis purified air. To ascertain the impact of variations in isotopologues on CO_2 measurements, we compared the isotopic bias between experimental values and theoretical calculations, whereas isotopic correction for CH_4 is estimated to be marginal. The isotopic bias from these two methods agreed well within the experimental error, suggesting that the isotopic bias can be corrected accurately by the theoretical calculation based on CO_2 stable isotope ratios. Using a sample humidification unit, we derived water correction functions for CO_2 and CH_4 from three different WS-CRDS instruments. Although the transferability of the correction functions among different WS-CRDS models was not clear, due to the relatively large uncertainty associated with the experiments, we observed no significant differences in the water correction values among the instruments at water vapor concentrations < 0.3 %V for CO_2 and < 0.4 %V for CH_4. These results suggest that complete dehumidification or moderate dehumidification followed by application of a water correction function is the best strategy for obtaining highly accurate CO_2 and CH_4 measurements, along with calibration with natural air-based standard gases or purified air-balanced synthetic standard gases with isotopic correction.

Acknowledgements. We thank T. Machida for his logistical support of our experiments. We are grateful to Y. Takahashi for CO_2 isotopic analysis. We also thank Y. Morino for valuable comments on our study. This study was conducted with financial support from the Ministry of the Environment, Japan as a Global Environment Research Account for National Institutes. Funding was also provided by the Global Environment Research Fund of the Ministry of the Environment, Japan (S-7-1).

References

Allison, C. E. and Francey, R. J.: Verifying Southern Hemisphere trends in atmospheric carbon dioxide stable isotopes, J. Geophys. Res., 112, D21304, doi:10.1029/2006JD007345, 2007.

Aydin, M., Verhulst, K. R., Saltzman, E. S., Battle, M. O., Monzka, S. A., Blake, D. R., Tang, Q., and Prather, M. J.: Recent decreases in fossil-fuel emissions of ethane and methane derived from firn air, Nature, 476, 198–202, doi:10.1038/nature10352, 2011.

Bischof, W.: The influence of the carrier gas on the infrared gas analysis of atmospheric CO_2, Tellus, 27, 59–61, 1975.

Brown, S. S.: Absorption spectroscopy in high-finesse cavities for atmospheric studies, Chem. Rev., 103, 5219–5238, 2003.

Buchwitz, M., de Beek, R., Burrows, J. P., Bovensmann, H., Warneke, T., Notholt, J., Meirink, J. F., Goede, A. P. H., Bergamaschi, P., Körner, S., Heimann, M., and Schulz, A.: Atmospheric methane and carbon dioxide from SCIAMACHY satellite data: initial comparison with chemistry and transport models, Atmos. Chem. Phys., 5, 941–962, doi:10.5194/acp-5-941-2005, 2005.

Chen, H., Winderlich, J., Gerbig, C., Hoefer, A., Rella, C. W., Crosson, E. R., Van Pelt, A. D., Steinbach, J., Kolle, O., Beck, V., Daube, B. C., Gottlieb, E. W., Chow, V. Y., Santoni, G. W., and Wofsy, S. C.: High-accuracy continuous airborne measurements of greenhouse gases (CO_2 and CH_4) using the cavity ring-down spectroscopy (CRDS) technique, Atmos. Meas. Tech., 3, 375–386, doi:10.5194/amt-3-375-2010, 2010.

Coplen, T. B., Bohlke, J. K., De Bievre, P., Ding, T., Holden, N. E., Hopple, J. A., Krouse, H. R., Lamberty, A., Peiser, H. S., Revesz, K., Rieder, S. E., Rosman, K. J. R., Roth, E., Taylor, P. D. P., Vocke, R. D., and Xiao, Y. K.: Isotope-abundance variations of selected elements (IUPAC Technical Report), Pure Appl. Chem., 74, 1987–2017, 2002.

Crosson, E. R.: A cavity ring-down analyzer for measuring atmospheric levels of methane, carbon dioxide, and water vapor, Appl. Phys. B-Lasers O., 92, 403–408, 2008.

Dicke, R.: The effect of collisions upon the Doppler width of spectral lines, Phys. Rev., 89, 472–473, 1953.

Galatry, L.: Simultaneous effect of Doppler and foreign gas broadening on spectral lines, Phys. Rev., 122, 1218–1223, 1961.

GLOBALVIEW-CO2C13: Cooperative Atmospheric Data Integration Project – δ^{13}C of Carbon Dioxide, CD-ROM, NOAA ESRL, Boulder, Colorado, available at: ftp://ftp.cmdl.noaa.gov/path: /ccg/co2c13/GLOBALVIEW (last access date: 12 July 2012), 2009.

Griffith, D. W. T.: Calculations of carrier gas effects in non-dispersive infrared analyzers, I. Theory, Tellus, 34, 376–384, 1982.

Griffith, D. W. T., Keeling, C. D., Adams, J. A., Guenther, P. R., and Bacastow, R. B.: Calculations of carrier gas effects in non-dispersive infrared analyzers, II. comparisons with experiment, Tellus, 34, 385–397, 1982.

Heimann, M.: Searching out the sinks, Nat. Geosci., 2, 3–4, doi:10.1038/ngeo405, 2009.

Kai, F. M., Tyler, S. C., Randerson, J. T., and Blake, D. R.: Reduced methane growth rate explained by decreased Northern Hemisphere microbial sources, Nature, 476, 194–197, doi:10.1038/nature10259, 2011.

Kozlova, E. A. and Manning, A. C.: Methodology and calibration for continuous measurements of biogeochemical trace gas and O_2 concentrations from a 300-m tall tower in central Siberia, Atmos. Meas. Tech., 2, 205–220, doi:10.5194/amt-2-205-2009, 2009.

Machida, T., Matsueda, H., Sawa, Y., Nakagawa, Y., Hirotani, K., Kondo, N., Goto, K., Nakazawa, T., Ishikawa, K., and Ogawa, T.: Worldwide measurements of atmospheric CO_2

and other trace gas species using commercial airlines, J. Atmos. Ocean. Technol., 25, 1744–1754, 2008.

Marquis, M. and Tans, P.: Carbon crucible, Science, 320, 460–461, 2008.

Messerschmidt, J., Geibel, M. C., Blumenstock, T., Chen, H., Deutscher, N. M., Engel, A., Feist, D. G., Gerbig, C., Gisi, M., Hase, F., Katrynski, K., Kolle, O., Lavrič, J. V., Notholt, J., Palm, M., Ramonet, M., Rettinger, M., Schmidt, M., Sussmann, R., Toon, G. C., Truong, F., Warneke, T., Wennberg, P. O., Wunch, D., and Xueref-Remy, I.: Calibration of TCCON column-averaged CO_2: the first aircraft campaign over European TCCON sites, Atmos. Chem. Phys., 11, 10765–10777, doi:10.5194/acp-11-10765-2011, 2011.

Montzka, S. A., Dolugokencky, E. J., and Butler, J. H.: Non-CO_2 greenhouse gases and climate change, Nature, 476, 43–50, doi:10.1038/nature10322, 2011.

Nakamichi, S., Kawaguchi, Y., Fukuda, H., Enami, S., Hashimoto, Satoshi, Kawasaki, M., Umekawa, T., Morino, I., Suto, H., Inoue, G.: Buffer-gas pressure broadening for the $(3\ 0^0\ 1)_{III} \leftarrow (0\ 0\ 0)$ band of CO_2 measured with continuous-wave cavity ring-down spectroscopy, Phys. Chem. Chem. Phys., 8, 364–368, 2006.

O'Keefe, A. and Deacon, A., G.: Cavity ring-down optical sectrometer for absorption measurements using pulsed laser sources, Rev. Sci. Instrum., 59, 2544–2554, 1988.

Pearman, G. I. and Garratt, J. R.: Errors in atmospheric CO_2 concentration measurements arising from the use of reference gas mixtgures different in composition to the sample air, Tellus, 27, 62–66, 1975.

Quay, P. D., Stutsman, J., Wilbur, D., Snover, A., Dlugokencky, E., and Brown, T.: The isotopic composition of atmospheric methane, Global Biogeochem. Cy., 13, 445–461, 1999.

Rella, C.: Accurate Greenhouse Gas Measurements in Humid Gas Streams Using the Picarro G1301 Carbon Dioxide/Methane/Water Vapour Gas Analyzer, PICARRO white paper, available at: http://www.picarro.com/resources/whitepapers/accurate_greenhouse_gas_measurements_in_humid_gas_streams_using_the_picarro_g1301_carbon_dio (last access: 12 July 2012), 2010.

Saitoh, N., Imasu, R., Ota, Y., and Niwa, Y.: CO_2 retrieval algorithm for the thermal infrared spectra of the greenhouse gases observing satellite: potential of retrieving CO_2 vertical profile from high-resolution FTS sensor, J. Geophys. Res., 114, D17305, doi:10.1029/2008JD011500, 2009.

Snover, A., Quay, P. D., and Hao, W. M.: The D/H content of methane emitted from biomass burning, Global Biogeochem. Cy., 14, 11–24, 2000.

Tohjima, Y.: Method for measuring changes in the atmospheric O_2/N_2 ratio by a gas chromatograph equipped with a thermal conductivity detector, J. Geophys. Res., 105, 14575–14584, 2000.

Tohjima, Y., Machida, T., Watai, T., Akama, I., Amari, T., and Moriwaki, Y.: Preparation of gravimetric standards for measurements of atmospheric oxygen and reevaluation of atmospheric oxygen concentration, J. Geophys. Res., 110, D11302, doi:10.1029/2004JD005595, 2005.

Tohjima, Y., Katsumata, K., Morino, I., Mukai, H., Machida, T., Akama, I., Amari, T., and Tsunogai, U.: Theoretical and experimental evaluation of the isotope effect of NDIR analyzer on atmospheric CO_2 measurement, J. Geophys. Res., 114, D13302, doi:10.1029/2009JD011734, 2009.

Varghese, P. and Hanson, R.: Collisional narrowing effects on spectral line shapes measured at high resolution, Appl. Opt., 23, 2376–2385, 1984.

Winderlich, J., Chen, H., Gerbig, C., Seifert, T., Kolle, O., Lavrič, J. V., Kaiser, C., Höfer, A., and Heimann, M.: Continuous low-maintenance $CO_2/CH_4/H_2O$ measurements at the Zotino Tall Tower Observatory (ZOTTO) in Central Siberia, Atmos. Meas. Tech., 3, 1113–1128, doi:10.5194/amt-3-1113-2010, 2010.

WMO: GAW Report No. 194 – 15th WMO/IAEA Meeting of Experts on Carbon Dioxide, Other Greenhouse Gases and Related Tracers Measurement Techniques, Tech. Rep., World Meteorological Organization, 2009.

Wunch, D., Toon, G. C., Blavier, J.-F., Washenfelder, R. A., Notholt, J., Connor, B. J., Griffith, D. W. T., Sherlock, V., and Wennberg, P. O.: The total carbon column observing network, Philos. T. Roy. Soc. A, 369, 2087–2112, doi:10.1098/rsta.2010.0240, 2012.

Xiong, X., Barnet, C. D., Zhuang, Q., Machida, T., Sweeney, C., Patra, P. K.: Mid-upper tropospheric methane in the high Northern Hemisphere: spaceborne observations by AIRS, aircraft measurements, and model simulations, J. Geophys. Res., 115, D19309, doi:10.1029/2009JD013796, 2010.

Yokota, T., Yoshida, Y., Eguchi, N., Ota, Y., Tanaka, T., Watanabe, H., Maksyutov, S.: Global concentrations of CO_2 and CH_4 retrieved from GOSAT: first preliminary results, SOLA, 5, 160–163, doi:10.2151/sola.2009-041, 2009.

Yoshida, Y., Ota, Y., Eguchi, N., Kikuchi, N., Nobuta, K., Tran, H., Morino, I., and Yokota, T.: Retrieval algorithm for CO_2 and CH_4 column abundances from short-wavelength infrared spectral observations by the Greenhouse gases observing satellite, Atmos. Meas. Tech., 4, 717–734, doi:10.5194/amt-4-717-2011, 2011.

Table 1. Calculated difference of pressure-broadening coefficients for O_2 and Ar from the coefficient of N_2 for CO_2 and CH_4*.

Model	Inert gas	Delta coefficient ($\Delta\varepsilon$)	
		$CO_2 \times 10^7$	$CH_4 \times 10^8$
EnviroSense 3000i	O_2	1.18 (0.01)	2.77 (0.6)
	Ar	2.10 (0.11)	5.67 (0.55)
G-1301	O_2	1.13 (0.1)	2.62 (0.06)
	Ar	1.82 (0.7)	6.44 (0.48)
G-2301	O_2	1.14 (0.01)	2.36 (0.07)
	Ar	1.88 (0.08)	5.67 (0.55)

* Numbers in parentheses are standard errors of the corresponding delta coefficients estimated by the linear least-squares analysis.

Table 2. Comparison of experimental and theoretical isotopic correction values[a].

Sample gas	NDIR	$\delta^{13}C/\delta^{18}O$ (‰)	Isotopic correction for NDIR[b]	WS-CRDS	PBE correction for WS-CRDS[c] (NDIR – WS-CRDS)	Experimental isotopic correction value	Calculated isotopic correction value	Experimental – theoretical
Compressed ambient air	402.15 ± 0.02	−9.07 ± 0.01 −2.29 ± 0.02	+0.11	402.12 ± 0.04	+0.01	0.13 ± 0.04	0.13 ± 0.07	0 ± 0.08
Synthetic STD 1	383.23 ± 0.01	−28.69 ± 0.01 −27.39 ± 0.02	+0.01	383.23 ± 0.05	+0.02	−0.01 ± 0.05	0 ± 0.07	−0.01 ± 0.08
Synthetic STD 2	369.79 ± 0.01	57.09 ± 0.02 −28.46 ± 0.02	+0.36	369.73 ± 0.04	+0.04	0.38 ± 0.04	0.35 ± 0.07	0.03 ± 0.08

[a] Values for CO_2 mole fraction are given in ppm.

[b] The correction values were calculated according to the method reported by Tohjima et al. (2009).

[c] The correction values were calculated on the basis of our results (see Sect. 3.2).

The background gas composition was determined by Tohjima et al. (2000).

Table 3. Water correction functions for three different WS-CRDS instruments along with the correction functions from past studies.

Group	Instrument model	CO_2: linear (10^{-2})/ quadratic (10^{-4}) terms	CH_4: linear (10^{-2})/ quadratic (10^{-4}) terms	Water vapor range (%V)
Chen et al. (2010)	G-1301	−1.20/−2.67	−0.98/−2.39	0.6–6
Winderlich et al. (2010)	EnviroSense 3000i	−1.205 ± 0.002/ −2.03 ± 0.08	−1.007 ± 0.005/ −1.45 ± 0.18	0–4
This study	EnviroSense 3000i	−1.207 ± 0.004/ −2.4 ± 0.1	−0.999 ± 0.007/ −2.1 ± 0.2	0.15–4.45
	G-1301	−1.204 ± 0.007/ −2.5 ± 0.2	−0.999 ± 0.013/ −1.4 ± 0.4	
	G-2301	−1.216 ± 0.009/ −1.6 ± 0.3	−0.968 ± 0.008/ −2.3 ± 0.2	

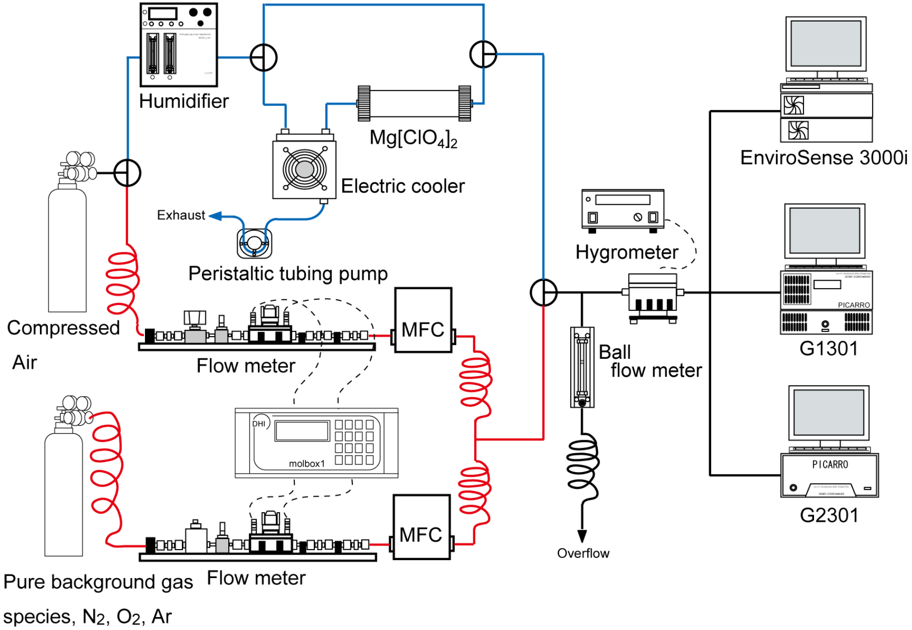

Fig. 1. Schematic diagram of the experimental system. The system consists of a sample humidification unit and a dynamic gas blending unit. Compressed air is supplied to the WS-CRDS instruments after adjustment of water vapor concentration via the humidification unit (blue line), while the mole fraction of the background gas in the sample air is adjusted through the dynamic gas blending unit (red line). See more detail in the text.

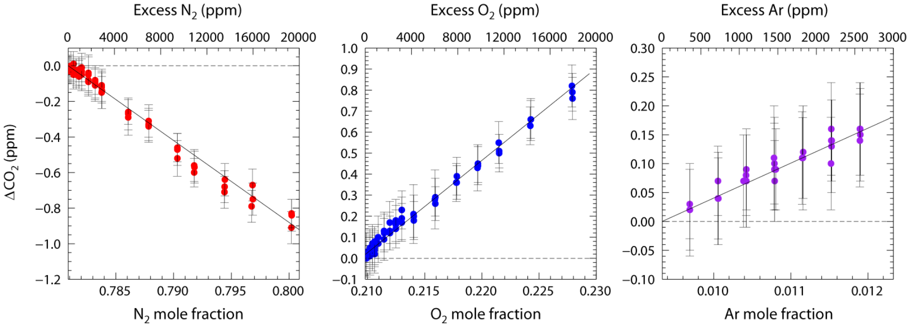

Fig. 2. Relationship between excess mole fraction of inert gases relative to their ambient levels and the resulting pressure-broadening effects on CO_2 measurements for WS-CRDS model G-1301. For each plot, the bottom axis indicates the increase in the amount of added inert gas in the sample air relative to the gas's ambient level, and the top axis indicates the relative increase in inert gas with respect to the bottom axis. The vertical bars in each plot denote the standard deviation ($\pm 1\sigma$) determined from the precision of WS-CRDS measurements and the flow meter. Errors in the calculation of N_2, O_2, and Ar mole fraction are less than 250, 135, and 61 ppm, respectively. The solid line is the relationship between the changes in matrix gas composition resulting from the inert gas addition and pressure-broadening effects, as calculated by linear least-squares analysis.

Title Page
Abstract
Introduction
Conclusions
References
Tables
Figures
◀▮
▶▮
◀
▶
Back
Close
Full Screen / Esc
Printer-friendly Version
Interactive Discussion

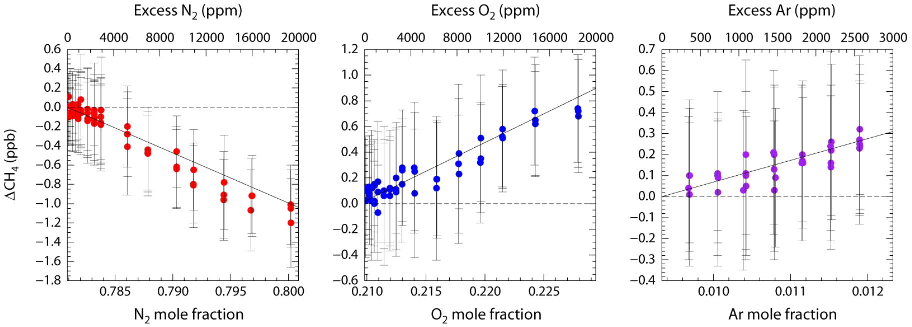

Fig. 3. The same as Fig. 2, but for CH_4.

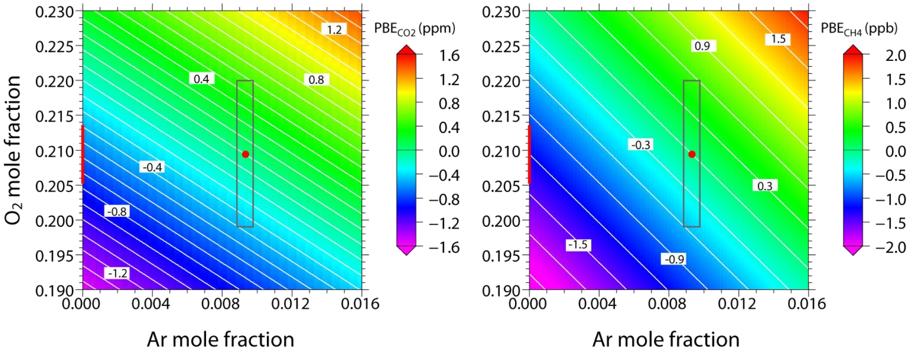

Fig. 4. Estimated pressure-broadening effects resulting from variations in matrix gas composition as a function of O_2 and Ar mole fraction for CO_2 measurements at 400 ppm (left) and for CH_4 measurements at 2000 ppb (right). The red circles denote ambient levels of O_2 and Ar. The gray solid rectangle denotes the ±5 % range of O_2 and Ar relative to their ambient levels. The thick red line on the y-axis indicates O_2 variation within ±2 % from its ambient level. The error associated with these estimations is negligible (less than 1 % of the estimated values).

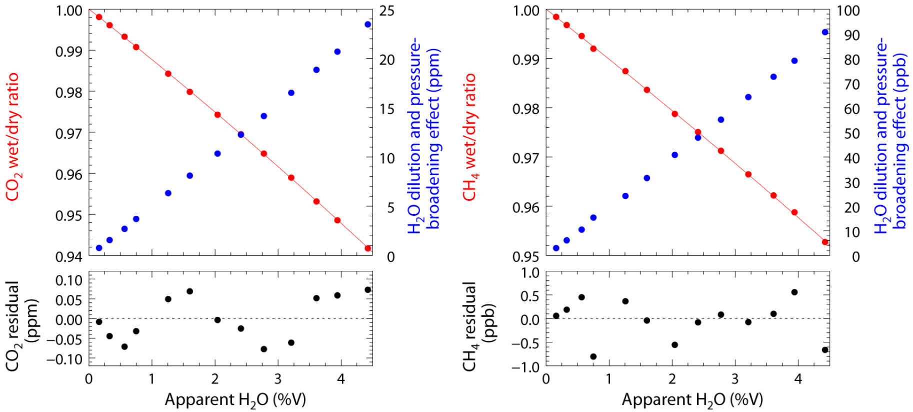

Fig. 5. The response of CO_2 and CH_4 against apparent water vapor concentration (values obtained from WS-CRDS measurements, model G-1301) along with the residuals from the fitting functions. The wet/dry ratio (left y-axis) indicates the ratio of the measured mixing ratio of the target gases in the wet and dry sample air, and the corresponding water vapor dilution and pressure-broadening effects (right y-axis) are defined as the difference between the dry and wet mixing ratios of the target gases. The solid red lines are fitting curves for the wet/dry ratios with parameters listed in Table 3.

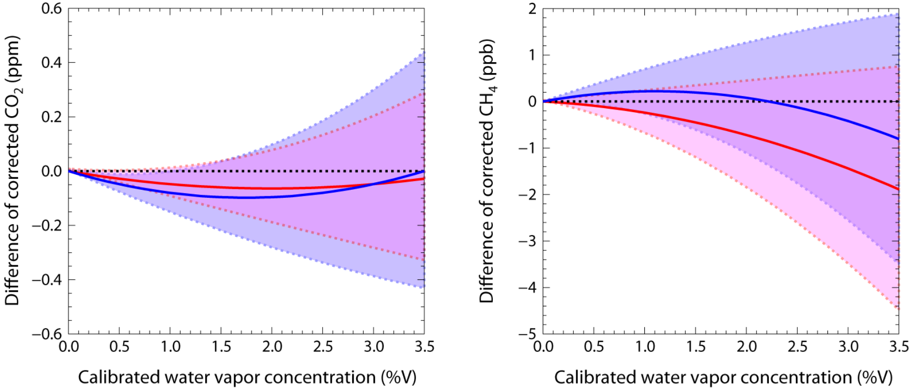

Fig. 6. Difference in the estimated water vapor correction values for CO_2 (left) and CH_4 (right) among the water vapor correction functions for three WS-CRDS models, plotted as a function of calibrated water vapor concentration. Red and blue solid lines indicate the difference between the EnviroSense 3000i and G-1301, and between G-2301 and G-1301, respectively. The dashed lines of corresponding colors indicate $\pm 1\sigma$ lines of the difference, and the $\pm 1\sigma$ regions are shaded with the corresponding colors.